

# Comparison between Three Promising $\beta^-$ -emitting Radionuclides, $^{67}\text{Cu}$ , $^{47}\text{Sc}$ and $^{161}\text{Tb}$ , with Emphasis on Doses Delivered to Minimal Residual Disease

Christophe Champion<sup>1</sup>✉, Michele A. Quinto<sup>1</sup>, Clément Morgat<sup>2</sup>, Paolo Zanotti-Fregonara<sup>2</sup>, Elif Hindie<sup>2</sup>✉

1. Université de Bordeaux, CNRS/IN2P3, Centre d'Etudes Nucléaires de Bordeaux Gradignan (CENBG), France;

2. Service de Médecine Nucléaire - CHU de Bordeaux; UMR-CNRS 5287; LabEx TRAIL; Université de Bordeaux, FRANCE.

✉ Corresponding authors: Pr Christophe Champion, PhD. Centre d'Etudes Nucléaires de Bordeaux Gradignan, Chemin du Solarium, BP 120, 33175 Gradignan. Tel.: +33 557120896; Fax: +33 557120801 e-mail: champion@cenbg.in2p3.fr Or Pr Elif Hindie, MD, PhD. Service de Médecine Nucléaire, Hôpital Haut-Lévêque, CHU de Bordeaux, 33604 Pessac, France. Tel: +(33)557656838; Fax: +(33)557656839 e-mail: elif.hindie@chu-bordeaux.fr.

© Ivyspring International Publisher. Reproduction is permitted for personal, noncommercial use, provided that the article is in whole, unmodified, and properly cited. See <http://ivyspring.com/terms> for terms and conditions.

Received: 2016.01.29; Accepted: 2016.05.01; Published: 2016.06.18

## Abstract

**PURPOSE:** Radionuclide therapy is increasingly seen as a promising option to target minimal residual disease. Copper-67, scandium-47 and terbium-161 have a medium-energy  $\beta^-$  emission which is similar to that of lutetium-177, but offer the advantage of having diagnostic partner isotopes suitable for pretreatment imaging. The aim of this study was to compare the efficacy of  $^{67}\text{Cu}$ ,  $^{47}\text{Sc}$  and  $^{161}\text{Tb}$  to irradiate small tumors.

**METHODS:** The absorbed dose deriving from a homogeneous distribution of  $^{67}\text{Cu}$ ,  $^{47}\text{Sc}$  or  $^{161}\text{Tb}$  in water-density spheres was calculated with the Monte Carlo code CELLDOSE. The diameters of the spheres ranged from 5 mm to 10  $\mu\text{m}$ , thus simulating micrometastases or single tumor cells. All electron emissions, including  $\beta^-$  spectra, Auger and conversion electrons were taken into account. Because these radionuclides differ in electron energy per decay, the simulations were run assuming that 1 MeV was released per  $\mu\text{m}^3$ , which would result in a dose of 160 Gy if totally absorbed.

**RESULTS:** The absorbed dose was similar for the three radionuclides in the 5-mm sphere (146–149 Gy), but decreased differently in smaller spheres. In particular,  $^{161}\text{Tb}$  delivered higher doses compared to the other radionuclides. For instance, in the 100- $\mu\text{m}$  sphere, the absorbed dose was 24.1 Gy with  $^{67}\text{Cu}$ , 14.8 Gy with  $^{47}\text{Sc}$  and 44.5 Gy with  $^{161}\text{Tb}$ . Auger and conversion electrons accounted for 71% of  $^{161}\text{Tb}$  dose. The largest dose differences were found in cell-sized spheres. In the 10- $\mu\text{m}$  sphere, the dose delivered by  $^{161}\text{Tb}$  was 4.1 times higher than that from  $^{67}\text{Cu}$  and 8.1 times that from  $^{47}\text{Sc}$ .

**CONCLUSION:**  $^{161}\text{Tb}$  can effectively irradiate small tumors thanks to its decay spectrum that combines medium-energy  $\beta^-$  emission and low-energy conversion and Auger electrons. Therefore  $^{161}\text{Tb}$  might be a better candidate than  $^{67}\text{Cu}$  and  $^{47}\text{Sc}$  for treating minimal residual disease in a clinical setting.

Key words: Dose, radionuclide therapy, minimal residual disease, micrometastases, terbium-161, copper-67, scandium-47, lutetium-177.

## Introduction

Targeted radionuclide therapy relies on the administration of radiolabeled compounds to irradiate tumors [1]. Iodine-131 has been used since seven decades to prevent recurrence of thyroid cancer

after surgery and to treat distant metastases [2–4]. In the past years, several other tumor-targeting radiopharmaceuticals, labeled with iodine-131, yttrium-90, or lutetium-177, have successfully entered

into clinical practice. Examples include  $^{131}\text{I}$ -MIBG for neural crest tumors, anti-CD20 antibodies (e.g.  $^{90}\text{Y}$ -ibritumomab tiuxetan) for lymphomas [5], the somatostatin analogs  $^{90}\text{Y}$ -DOTATOC and  $^{177}\text{Lu}$ -DOTATATE for neuroendocrine tumors [6] and more recently  $^{177}\text{Lu}$ -labelled PSMA ligands for metastatic prostate cancer [7]. Notably, an ever-increasing number of preclinical studies and clinical trials aim at using radionuclide therapy to treat minimal residual disease: *i.e.* as adjuvant therapy or for consolidation after remission [8-13].

Many of the novel radiopharmaceuticals for targeted therapy have been armed with lutetium-177 [6-9].  $^{177}\text{Lu}$  can be stably chelated to various peptides and antibodies [14]. Compared to the high-energy electrons of  $^{90}\text{Y}$ , the medium-energy  $\beta^-$  emission of  $^{177}\text{Lu}$  allows for a more effective irradiation of small tumors and is associated with a reduced non-specific toxicity [15-18]. Both characteristics are important in the perspective of targeting minimal residual disease. Moreover,  $^{177}\text{Lu}$  emits  $\gamma$  photons which enable post-therapy imaging.

Three other promising medium-energy  $\beta^-$  emitters are: copper-67 [19,20], scandium-47 [21,22] and terbium-161 [23-25]. Their half-lives are suitable for targeted radionuclide therapy with peptides and antibodies (Table 1). The half-life of  $^{161}\text{Tb}$  (6.91 d) is similar to that of  $^{177}\text{Lu}$  (6.65 d). The half-lives of  $^{67}\text{Cu}$  and  $^{47}\text{Sc}$  are shorter (respectively 2.58 d and 3.35 d) and thus they might be used to label molecules that exhibit a more rapid washout from tumor tissues. Just like  $^{177}\text{Lu}$ ,  $^{161}\text{Tb}$  is a radiolanthanide that can be stably linked to various molecules using for example DOTA as chelator [24,25]. Chelators that are suitable for stable coordination of copper and scandium are also available [14]. All three radionuclides are amenable to imaging thanks to some gamma photon emissions (Table 1). Photons from  $^{67}\text{Cu}$  and  $^{47}\text{Sc}$  (184.6 keV and 159.4 keV, respectively) are better suited to post-therapy imaging with gamma cameras than the

photons emitted by  $^{161}\text{Tb}$  (whose energy of 74.6 keV is similar to that emitted by the myocardial imaging agent  $^{201}\text{Tl}$ ). On the other hand, the lower proportion of photon emission of  $^{161}\text{Tb}$  (~15% of the total emitted energy, compared to ~40% for  $^{67}\text{Cu}$  or  $^{47}\text{Sc}$ ) minimizes total body dose and allows for treatment on an outpatient basis.

One major advantage of these radionuclides over  $^{177}\text{Lu}$  is the theranostic potential, *i.e.* the availability of  $\beta^+$  ( $^{64}\text{Cu}$ ,  $^{43}\text{Sc}$ ,  $^{44}\text{Sc}$ ,  $^{152}\text{Tb}$ ) or  $\gamma$ -emitting ( $^{155}\text{Tb}$ ) radioisotopes that enable PET or SPECT pre-therapy imaging and dosimetry [26-30]. Table 2 summarizes the physical properties of these diagnostic radionuclides. The biodistribution of the molecule labeled with the diagnostic radionuclide is expected to faithfully match that of the therapeutic molecule.

The aim of this study was to compare the effectiveness of  $^{67}\text{Cu}$ ,  $^{47}\text{Sc}$  and  $^{161}\text{Tb}$  at irradiating small tumors. Using the Monte Carlo code CELLDOS [31,32], we assessed the dose deposits from these radionuclides in spheres of various sizes, simulating micrometastases and single tumor cells.

## Methods

The absorbed dose in each sphere was assessed with Monte Carlo simulations by taking into account all electron emissions:  $\beta^-$ -spectra, conversion electrons (CE) and Auger electrons (including Coster-Kronig electrons). Emission data were obtained from the International Commission on Radiological Protection (ICRP) publication ICRP-107 [30]. Photons were neglected. For all simulations, the distribution of radioactivity within spheres was assumed to be homogeneous. This was achieved by random Monte Carlo sampling throughout the sphere volume using a high number of simulations ( $\geq 1,000,000$  per sphere). Decay characteristics of  $^{67}\text{Cu}$ ,  $^{47}\text{Sc}$  and  $^{161}\text{Tb}$  are reported in Table 1. The spectra of electron emissions are shown in Figure 1.

**Table 1:** Radionuclide characteristics (see also Figure 1 for electron emission spectra).

Radionuclide	$^{67}\text{Cu}$	$^{47}\text{Sc}$	$^{161}\text{Tb}$
Half-life (day)	2.576	3.349	6.906
Type of Decay (%)	$\beta^-$ (100 %)	$\beta^-$ (100 %)	$\beta^-$ (100 %)
$\beta$ particles mean energy (keV)	135.9	161.9	154.3
Daughter	$^{67}\text{Zinc}$ (stable)	$^{47}\text{Titanium}$ (stable)	$^{161}\text{Dysprosium}$ (stable)
CE emission (energy per decay in keV)	13.74	0.48	39.28
CE energy range (keV) *	81.6 – 184.5	154.4 – 158.9	3.3 – 98.3
Auger and Coster-Kronig electrons (energy per decay in keV)	0.75	0.01	8.94
Auger and Coster-Kronig electrons energy range (keV) *	0.057 – 9.4	0.027 – 4.8	0.018 – 50.9
Total electron energy per decay (average in keV)	150.4	162.4	202.5
$\gamma$ radiation useful for imaging (Energy in keV and % abundance)	184.6 (49.6%); 91.3 (7.6%); 93.3 (3%)	159.4 (68.3%)	74.6 (10.2%)
Photons X and $\gamma$ (total energy per decay in keV)	114.9	108.9	36.35
Energy per decay in keV (photons + electrons)	265.3	271.3	238.9
Percentage of energy emitted as photons	43.3 %	40.1 %	15.2 %

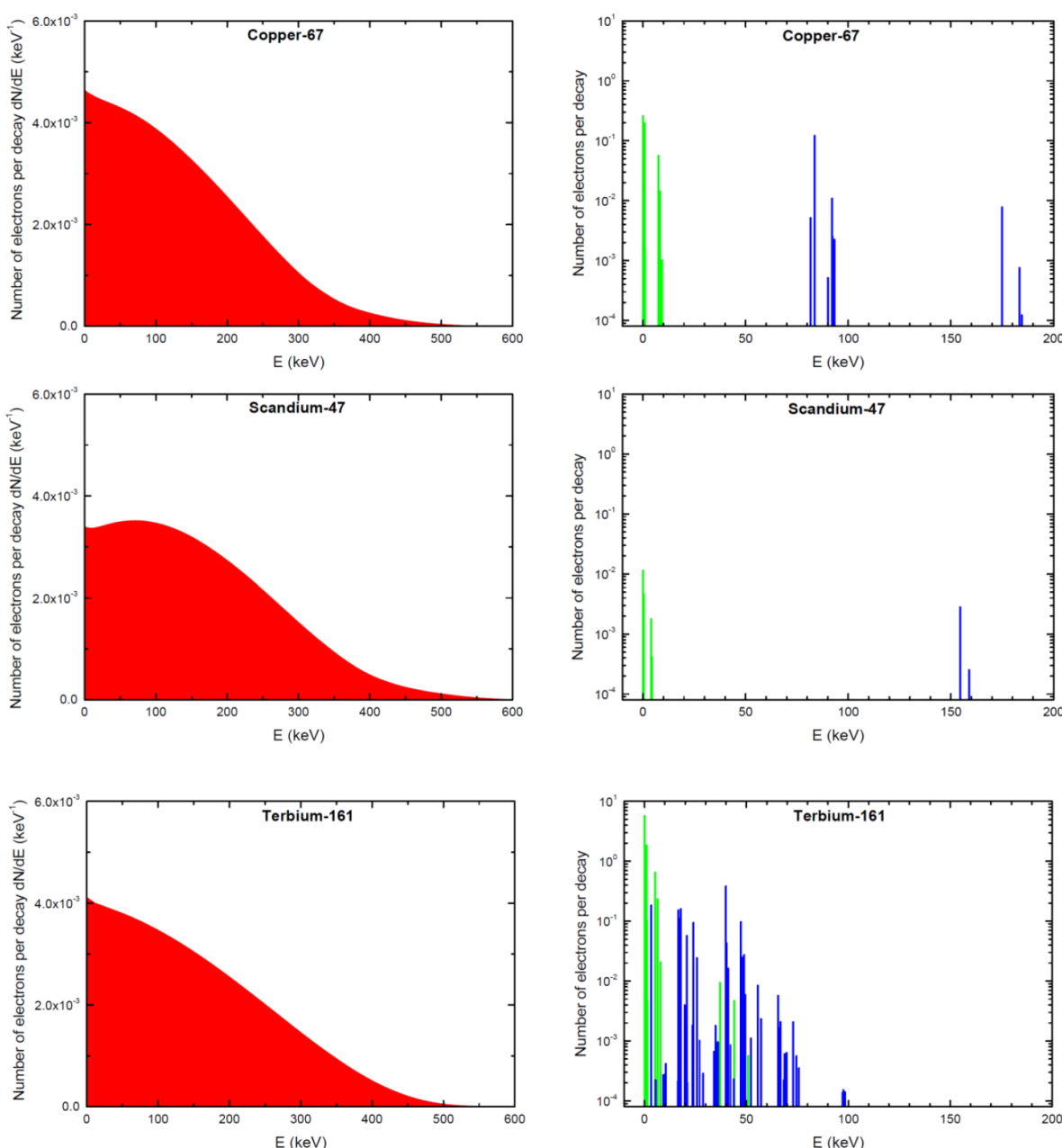
\* Conversion and Auger electrons with probability <0.0001 were neglected (30).

**Table 2:** Physical characteristics of the diagnostic radionuclides  $^{64}\text{Cu}$ ,  $^{43}\text{Sc}$ ,  $^{44}\text{Sc}$ ,  $^{152}\text{Tb}$  and  $^{155}\text{Tb}$ .

Radionuclide	$^{64}\text{Cu}$	$^{43}\text{Sc}$	$^{44}\text{Sc}$	$^{152}\text{Tb}$	$^{155}\text{Tb}$
Half-life	12.7 h	3.89 h	3.97 h	17.5 h	5.32 days
Type of Decay	EC, $\beta^+$ , $\beta^-$ $\beta^+$ (17.6%), $\beta^-$ (38.5%)	EC, $\beta^+$ $\beta^+$ (88.1%)	EC, $\beta^+$ $\beta^+$ (94.3 %)	EC, $\beta^+$ $\beta^+$ (20.3%)	EC (100%)
Mean energy of $\beta$ particles (keV)	$\beta^+$ : 278 $\beta^-$ : 191	$\beta^+$ : 476	$\beta^+$ : 632	$\beta^+$ : 1140	-
Main $\gamma$ emissions ( $\geq 5\%$ )	-	372.9 keV (22.5%)	1157 keV (99.9%)	271.1 keV (9.5%) 344.3 keV (63.5%) 586.3 keV (9.2%) 778.9 keV (5.5%)	86.6 keV (32.0 %) 105.3 keV (25.1%) 180.1 keV (7.5%) 262.3 keV (5.3%)
X and $\gamma$ emission (total energy per decay in keV) §	~ 8	~ 85	~ 1177	~ 1146	~ 176

§ Photon emissions following  $\beta^+$  annihilation are not considered.

EC = Electron capture.

**Figure 1:** Electron emissions of  $^{67}\text{Cu}$ ,  $^{47}\text{Sc}$  and  $^{161}\text{Tb}$ .  $\beta$ -spectra are in red (integral of the curve = 1), conversions electrons (CE) are in blue and Auger electrons (including Coster-Kronig electrons) in green. Conversion and Auger electrons whose probability was  $<0.0001$  [30] were neglected and are not represented.

Event-by-event electron track simulations in CELLDPOSE are based on the cross sections of the interactions between the electron and the water molecule, and take into account ionizations, excitations and elastic scattering processes [31-33]. The slowing-down histories for primary and secondary electrons are described until the energy falls to 7.4 eV (electron excitation threshold of the water molecule) [33]. The residual energy is considered to be absorbed locally.

The doses from a single radioactive decay (S-values) for  $^{67}\text{Cu}$  and  $^{47}\text{Sc}$  were assessed in spheres of water density and compared with those previously calculated for  $^{161}\text{Tb}$  in the same spheres [18]. The diameter of the spheres ranged from 5 mm to 10  $\mu\text{m}$ , thus simulating micrometastases of various sizes and single tumor cells. The relative contribution from the different electron emissions ( $\beta^-$  particles, CE and Auger electrons) was also assessed as previously described with  $^{131}\text{I}$  [31].

In addition to S-values, we calculated the absorbed dose resulting from a uniform concentration of events (1 decay per  $\mu\text{m}^3$ ). Since  $^{67}\text{Cu}$ ,  $^{47}\text{Sc}$  and  $^{161}\text{Tb}$  differ in the total amount of electron energy emitted per decay, the absorbed doses were compared after normalization over a fixed amount of energy released per unit of volume (1 MeV per  $\mu\text{m}^3$ ). If totally absorbed, this concentration would yield 160 Gy. Based on the total electron energy per decay (Table 1), the average number of decays per cubic micrometer (N) that releases 1 MeV of energy is: 6.65 for  $^{67}\text{Cu}$ , 6.16 for  $^{47}\text{Sc}$  and 4.94 for  $^{161}\text{Tb}$ . Assuming a complete physical decay, no biological elimination, and a tissue density of 1 g/cm $^3$ , this corresponds to an activity concentration ( $A_0 = N \times \ln 2 / T$ ) of: 20.71 MBq/g for  $^{67}\text{Cu}$ , 14.76 MBq/g for  $^{47}\text{Sc}$  and 5.74 MBq/g for  $^{161}\text{Tb}$ .

Finally, we examined the spatial profile of energy deposits around a point source of  $^{67}\text{Cu}$ ,  $^{47}\text{Sc}$  or  $^{161}\text{Tb}$ . Energy deposits (eV per decay) were studied inside concentric 10- $\mu\text{m}$ -thick shells around the point source.

**Table 3:** S-values for  $^{67}\text{Cu}$ ,  $^{47}\text{Sc}$  and  $^{161}\text{Tb}$  and contribution of the different electronic emissions.

Sphere diameter ( $\mu\text{m}$ )	S-values (Gy.Bq $^{-1}.\text{s}^{-1}$ )			Contribution of the different electronic emissions								
				$^{67}\text{Cu}$				$^{47}\text{Sc}$				$^{161}\text{Tb}$
	$^{67}\text{Cu}$	$^{47}\text{Sc}$	$^{161}\text{Tb}$	$\beta^-$ (%)	CE (%)	Auger (%)	$\beta^-$ (%)	CE (%)	Auger (%)	$\beta^-$ (%)	CE (%)	Auger (%)
5,000	$3.37 \times 10^{-10}$	$3.69 \times 10^{-10}$	$4.47 \times 10^{-10}$	89.9	9.5	0.6	99.7	0.29	0.01	74.1	21.0	4.9
2,000	$4.67 \times 10^{-9}$	$4.74 \times 10^{-9}$	$6.22 \times 10^{-9}$	89.0	10.4	0.6	99.7	0.29	0.01	71.0	23.5	5.5
1,000	$3.07 \times 10^{-8}$	$2.77 \times 10^{-8}$	$4.14 \times 10^{-8}$	87.2	12.1	0.7	99.7	0.29	0.01	65.5	27.9	6.6
500	$1.77 \times 10^{-7}$	$1.40 \times 10^{-7}$	$2.54 \times 10^{-7}$	84.1	14.9	1.0	99.6	0.35	0.05	55.9	35.5	8.6
200	$1.52 \times 10^{-6}$	$1.05 \times 10^{-6}$	$2.76 \times 10^{-6}$	79.3	18.9	1.8	99.7	0.24	0.06	40.1	47.7	12.2
100	$6.89 \times 10^{-6}$	$4.58 \times 10^{-6}$	$1.71 \times 10^{-5}$	79.4	17.3	3.3	99.7	0.19	0.11	29.3	55.1	15.6
50	$2.95 \times 10^{-5}$	$1.95 \times 10^{-5}$	$1.02 \times 10^{-4}$	81.2	12.8	6.0	99.7	0.17	0.13	21.4	58.1	20.5
20	$2.12 \times 10^{-4}$	$1.30 \times 10^{-4}$	$9.70 \times 10^{-4}$	77.3	10.0	12.7	99.5	0.16	0.34	15.3	52.3	32.4
10	$9.80 \times 10^{-4}$	$5.38 \times 10^{-4}$	$5.41 \times 10^{-3}$	70.7	8.3	21.0	99.2	0.15	0.65	11.7	43.4	44.9

## Results

### S values for $^{67}\text{Cu}$ , $^{47}\text{Sc}$ and $^{161}\text{Tb}$ and contribution of the different electron emissions

S-values measured with the Monte-Carlo dose CELLDPOSE are reported in Table 3. Results agreed (differences <10%) with those reported by Bardiès for  $^{67}\text{Cu}$  and  $^{47}\text{Sc}$  in spheres >20  $\mu\text{m}$  using analytic methods based on scaled dose point kernel [34]. Bardiès and colleagues did not report on smaller spheres and did not study Terbium-161. The relative contributions of  $\beta^-$  particles, CE and Auger electrons are also reported in Table 3. In the case of  $^{47}\text{Sc}$ , almost all the absorbed dose was due to  $\beta^-$  emission (>99% for all spheres).  $\beta^-$  emission was also the main contributor to the doses delivered by  $^{67}\text{Cu}$ , with only modest contribution from CE and Auger electrons (10.1 to 29.3%). By contrast,  $^{161}\text{Tb}$  displayed a significant contribution from CE and Auger electrons. The combined contribution from  $^{161}\text{Tb}$  CE and Auger electrons to the total absorbed dose was 25.9% in the 5-mm sphere and reached 88.3% in the cell-sized 10- $\mu\text{m}$  sphere (Table 3).

### Electron dose deposits after normalization

When 1 MeV per  $\mu\text{m}^3$  was released, the absorbed dose in the 5-mm sphere was similar for the three radionuclides (146 to 149 Gy). The absorbed dose progressively decreased when the sphere size decreased, but the dose reduction was more abrupt for  $^{67}\text{Cu}$  and  $^{47}\text{Sc}$  than for  $^{161}\text{Tb}$  (Fig. 2).  $^{161}\text{Tb}$  was clearly superior to the other radionuclides for spheres with less than 1mm diameter. For example, in a 100- $\mu\text{m}$  micrometastasis the absorbed dose was 24.1 Gy with  $^{67}\text{Cu}$ , 14.8 Gy with  $^{47}\text{Sc}$  and 44.5 Gy with  $^{161}\text{Tb}$  (Table 4). The largest dose difference was found in cell-sized spheres: in the 10- $\mu\text{m}$  sphere, the doses delivered by  $^{67}\text{Cu}$ ,  $^{47}\text{Sc}$  and  $^{161}\text{Tb}$  were 3.42 Gy, 1.74 Gy and 14.1 Gy, respectively (Table 4).

**Table 4:** Absorbed dose from  $^{67}\text{Cu}$ ,  $^{47}\text{Sc}$ , and  $^{161}\text{Tb}$  assuming a uniform concentration of the radionuclide. Data for  $^{177}\text{Lu}$  are shown for comparison.

Sphere diameter ( $\mu\text{m}$ )	Absorbed dose for 1 decay per $\mu\text{m}^3$ (Gy)				Absorbed dose for 1 MeV released per $\mu\text{m}^3$ (Gy)				Absorbed dose ratio "Efficacy ratio" (with $^{177}\text{Lu}$ as reference) §			
	$^{177}\text{Lu}$	$^{67}\text{Cu}$	$^{47}\text{Sc}$	$^{161}\text{Tb}$	$^{177}\text{Lu}$	$^{67}\text{Cu}$	$^{47}\text{Sc}$	$^{161}\text{Tb}$	$^{177}\text{Lu}$	$^{67}\text{Cu}$	$^{47}\text{Sc}$	$^{161}\text{Tb}$
5,000	21.6	22.1	24.2	29.3	145	147	149	146	1	1.01	1.03	1.01
2,000	19.0	19.6	19.8	26.0	128	130	122	129	1	1.02	0.95	1.01
1,000	15.4	16.1	14.5	21.7	104	107	89.6	108	1	1.03	0.86	1.04
500	11.1	11.6	9.19	16.6	74.8	77.1	56.7	82.7	1	1.03	0.76	1.11
200	6.18	6.37	4.39	11.6	41.8	42.4	27.2	57.6	1	1.01	0.65	1.38
100	3.63	3.61	2.39	8.95	24.5	24.1	14.8	44.5	1	0.98	0.60	1.82
50	2.08	1.93	1.28	6.67	14.1	12.9	7.89	33.3	1	0.91	0.56	2.36
20	0.98	0.89	0.54	4.06	6.61	5.91	3.35	20.2	1	0.89	0.51	3.06
10	0.58	0.51	0.28	2.83	3.92	3.42	1.74	14.1	1	0.87	0.44	3.60

§ The absorbed doses from  $^{67}\text{Cu}$ ,  $^{47}\text{Sc}$  and  $^{161}\text{Tb}$  (dose for 1 MeV released per  $\mu\text{m}^3$ ) are divided by the doses from  $^{177}\text{Lu}$ , which is used as a reference.  $^{177}\text{Lu}$  data are taken from [18].

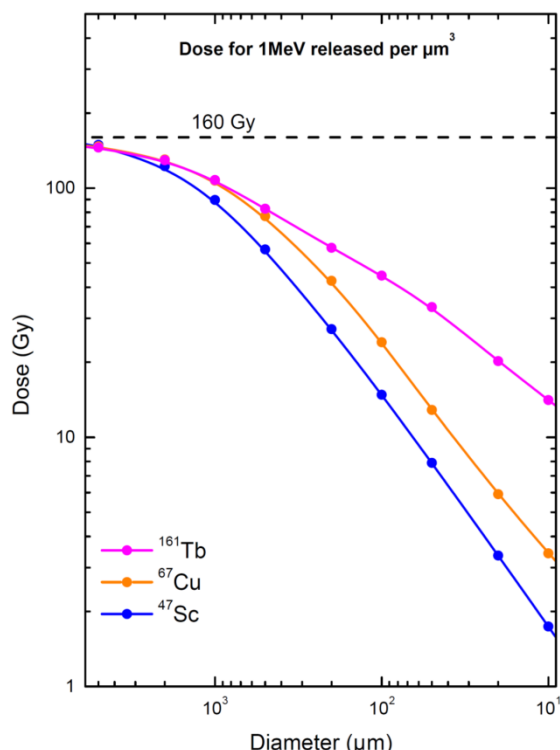


**Figure 2:** Electron dose delivered by  $^{67}\text{Cu}$ ,  $^{47}\text{Sc}$  and  $^{161}\text{Tb}$  (considering 1 MeV released per  $\mu\text{m}^3$ ) as a function of sphere size. The maximal value of 160 Gy/MeV/ $\mu\text{m}^3$  corresponds to total absorption.

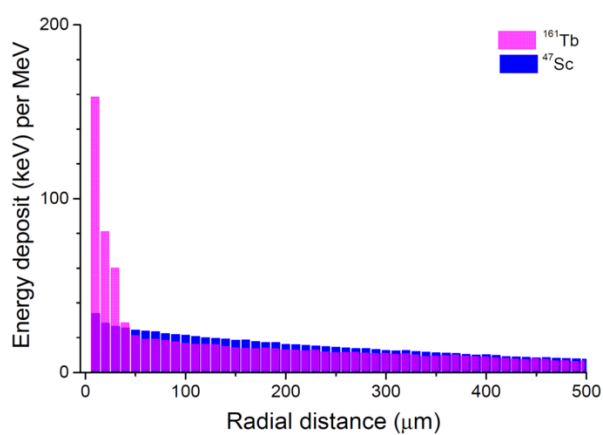


**Figure 3:** Patterns of energy deposit (keV per MeV released) of  $^{47}\text{Sc}$  and  $^{161}\text{Tb}$  over the first 500  $\mu\text{m}$  around a point source.

## Electron energy deposit around a point source

The energy deposited by  $^{161}\text{Tb}$  (per MeV released) was considerably higher than that deposited by the other radionuclides up to 30  $\mu\text{m}$  around the point source (Fig. 3). This suggests that  $^{161}\text{Tb}$  would deliver a higher dose not only to the targeted cell, but also to its immediate neighbors. Beyond this distance, the differences in energy deposits leveled off: the radius within which 50% of the energy is deposited (R50) was 0.17 mm for  $^{67}\text{Cu}$ , 0.25 mm for  $^{47}\text{Sc}$  and 0.15 mm for  $^{161}\text{Tb}$ . The radius within which 90% of the emitted energy is deposited (R90) was 0.57 mm for  $^{67}\text{Cu}$ , 0.72 mm for  $^{47}\text{Sc}$  and 0.63 mm for  $^{161}\text{Tb}$ .

## Discussion

In many cancers, the prognosis is linked to metastatic relapse, which may occur years after primary surgery [35-37]. Targeted radionuclide therapy may play a major role to treat occult micrometastases in high-risk patients or to eradicate minimal residual disease [2, 8-13]. Several preclinical and clinical studies suggest that radionuclide therapy is more effective when administered at an early stage of the disease [4, 6, 38, 39], probably because the distribution of the radiopharmaceutical in tumors is still relatively homogeneous. However, radionuclides differ in their ability to irradiate micrometastases [16]. In this study we assessed the relative effectiveness of three promising medium-energy  $\beta$ -emitters, *i.e.*  $^{67}\text{Cu}$ ,  $^{47}\text{Sc}$  and  $^{161}\text{Tb}$ .

Since the electron energy per decay of these three radionuclides differs, we assumed that 1 MeV was released per  $\mu\text{m}^3$ . If totally absorbed, this energy would always yield a dose of 160 Gy. Absorbed doses of this magnitude were measured in macrometastases of neuroendocrine tumors in patients who responded to  $^{177}\text{Lu}$ -DOTATATE therapy [40]. Smaller and more homogeneous tumors are expected to respond to lower doses.

Our simulations showed that, for the three radionuclides, the doses delivered to a 5-mm metastasis (146 to 149 Gy) were close to the dose that would result from total absorption. The doses decreased with sphere size, thus underscoring the fact that micrometastases are more difficult to irradiate effectively. The dose delivered by  $^{161}\text{Tb}$  was however consistently higher than that delivered by the other radionuclides (Fig. 2). For example, in a 100- $\mu\text{m}$  micrometastasis, the absorbed dose was 44.5 Gy for  $^{161}\text{Tb}$ , 24.1 Gy for  $^{67}\text{Cu}$  and 14.8 Gy for  $^{47}\text{Sc}$  (Table 4). The largest differences were found in the smallest spheres: in a cell-sized sphere of 10  $\mu\text{m}$  diameter, the dose delivered by  $^{161}\text{Tb}$  was 14.1 Gy, compared to 3.42 Gy and 1.74 Gy for  $^{67}\text{Cu}$  and  $^{47}\text{Sc}$ . Thus, relatively to the almost pure  $\beta^-$  emission of  $^{47}\text{Sc}$ , the doses delivered by  $^{161}\text{Tb}$  were  $\sim 3$  times higher in a 100- $\mu\text{m}$  micrometastasis and  $\sim 8$  times higher in a 10- $\mu\text{m}$  single cell (Table 4). In a previous work, we showed that the dose delivered by  $^{161}\text{Tb}$  to small metastases was also higher than that delivered by  $^{177}\text{Lu}$  [18]. In Table 4, the absorbed doses from  $^{67}\text{Cu}$ ,  $^{47}\text{Sc}$  and  $^{161}\text{Tb}$  (for 1 MeV released per  $\mu\text{m}^3$ ) are compared to those from  $^{177}\text{Lu}$ , used as a reference.

Our Monte Carlo study provides a mechanistic framework that explains some recent preclinical findings on tumor-control efficacy [24,25]. Anti-L1CAM antibody labeled with  $^{161}\text{Tb}$  inhibited the growth of subcutaneous xenografts of ovarian

cancer more effectively than the same antibody labeled with  $^{177}\text{Lu}$  and injected at a comparable activity (corresponding to 50% of the maximum tolerated dose) [25]. In a cell culture study, the radioactivity concentration of folate conjugates required to achieve the half-maximal inhibition of KB cells (human cervical carcinoma) was 4.5 fold lower with the  $^{161}\text{Tb}$ -labeled conjugate than with the  $^{177}\text{Lu}$ -labeled conjugate [24]. This difference was smaller ( $\times 1.7$ ) for IGROV-1 cells (human ovarian carcinoma), which might be explained by the lower internalization rate of folate conjugates into these cells [24].

The higher efficacy of  $^{161}\text{Tb}$  compared to  $^{47}\text{Sc}$  and  $^{67}\text{Cu}$  is mainly due to the larger amount of Auger and low-energy conversion electrons (Fig. 1), whose doses are deposited over relatively short distances (Fig. 4). Indeed, CE and Auger electrons accounted for 71% of the radiation dose deposited by  $^{161}\text{Tb}$  in a 100- $\mu\text{m}$  metastasis and 88% of the dose deposited in a 10- $\mu\text{m}$  cell (Table 3). This contrasts with  $^{47}\text{Sc}$  data, where >99% of the absorbed energy was due to  $\beta^-$  particles for all spheres. The interpretation of experimental results may be further refined by considering the linear energy transfer (LET) of emitted electrons. Not only emission spectra from  $^{161}\text{Tb}$  are rich in Auger electrons, but also the majority of conversion electrons of  $^{161}\text{Tb}$  have low energy (< 50 keV) and thus high LET (Table 5).

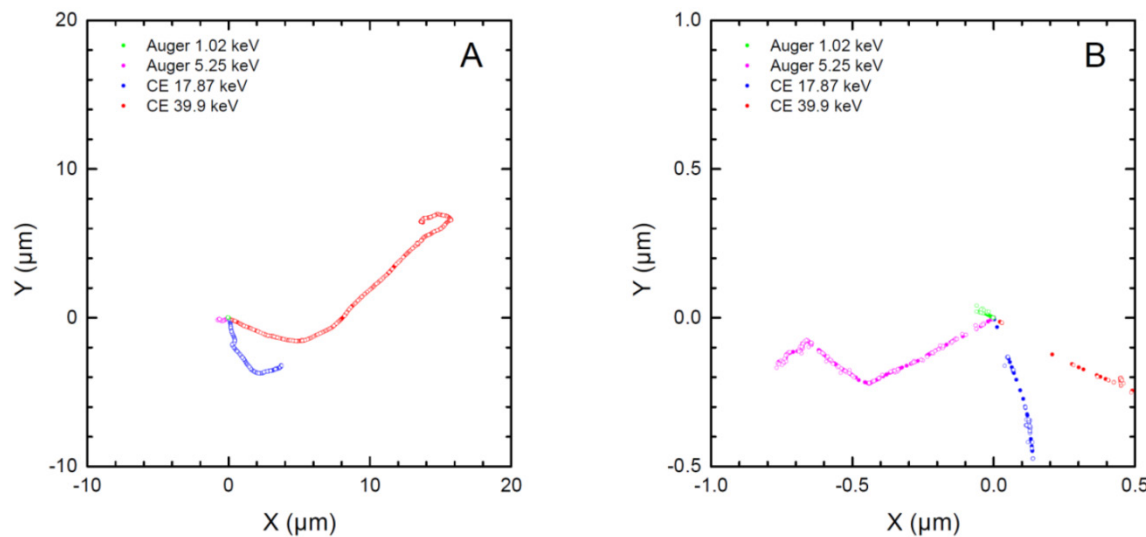


**Figure 4:** Two-dimensional plots of the tracks of two representative conversion electrons and two representative Auger electrons from  $^{161}\text{Tb}$  as simulated with CELLDOSE. Panel A reproduces the full path of the two CE (39.9 keV and 17.87 keV). Panel B is a magnification of the paths of Auger electrons (5.25 keV, 1.02 keV). The solid and open circles represent the ionizing interactions induced by the primary and the secondary electrons, respectively.

**Table 5:** Comparison between  $^{177}\text{Lu}$ ,  $^{67}\text{Cu}$ ,  $^{47}\text{Sc}$ , and  $^{161}\text{Tb}$ : Energy released as Auger and conversion electrons per decay (keV) and its distribution within specific energy ranges. The linear energy transfer (LET) for each energy category is also shown.

Energy range (keV)	LET § (keV/ $\mu\text{m}$ )	$^{177}\text{Lu}$	$^{67}\text{Cu}$	$^{47}\text{Sc}$	$^{161}\text{Tb}$
0.1 - 1	19.23 - 9.51	0.11	0.2	~ 0	1.3
1 - 10	9.51 - 2.26	0.89	0.55	0.01	7.7
10 - 50	2.26 - 0.66	2.6	-	-	37.5
50 - 200	0.66 - 0.28	11	13.7	0.48	1.6
Total energy per decay from Auger and conversion electrons (keV)	14.7		14.5	0.5	48.2

§ LET values for electrons  $\geq 10$  keV are taken from the database ESTAR [46]; the other LET values are from Champion [33]. The highest LET value is for electrons whose energy is close to 0.15 keV.

Knowledge of the biodistribution of the radiopharmaceutical at the cellular and subcellular level is of paramount importance to rationally choose the most appropriate radionuclide. Radionuclides can be imaged and quantified with techniques such as autoradiography or secondary ion mass microscopy [41]. This distribution may be used as input to derive the dose to tumor cells [32]. The energy deposited by  $^{161}\text{Tb}$  (per MeV released) is higher than that deposited by the other radionuclides up to 30  $\mu\text{m}$  around a point source (Fig. 3). Thus,  $^{161}\text{Tb}$  would likely deliver a higher dose, not only to the targeted cell, but also to its immediate neighbors. Moreover, the short tracks of energy deposit of Auger electrons and some low energy conversion electrons (Fig. 4) suggest that a putative  $^{161}\text{Tb}$ -labeled radiopharmaceutical would be even more effective if transported into the cell and internalized into the nucleus [42]. The impact of Auger electrons on other targets such as the cell membrane also deserves investigation [43]. Our future work will compare the dose distribution of  $^{161}\text{Tb}$  to that of other  $\beta$ -, Auger- or  $\alpha$ -emitting radionuclides [44] for various cellular distributions. Also, since only limited preclinical work on  $^{161}\text{Tb}$  has been done so far [24,25], additional studies should be carried out to establish whether  $^{161}\text{Tb}$  is a good candidate for clinical use. Hopefully, preclinical data [24,25], and the theoretical framework provided by our own calculations, will encourage the development of new radiopharmaceuticals labelled with  $^{161}\text{Tb}$ .

Finally, the choice of radionuclides for radiopharmaceutical therapy may be driven by logistic issues. Producing  $^{67}\text{Cu}$  as no-carrier-added in amounts suitable for large clinical use has been difficult [19,20]. The optimal technique to produce  $^{47}\text{Sc}$  is still debated [21,22]. Preliminary data suggest that  $^{161}\text{Tb}$  can be produced in large amounts as no-carrier-added, using for example a gadolinium-160 target ( $^{160}\text{Gd}(\text{n},\gamma)^{161}\text{Tb}$ ), and with good radionuclide purity ( $^{160}\text{Tb}$  to  $^{161}\text{Tb}$  activity ratio  $<0.0001$ ) [45]. The cost for large-scale production is estimated to be comparable to that of no-carrier-added  $^{177}\text{Lu}$  [45].

## Conclusion

Radiopharmaceutical therapy can effectively target isolated tumor cells and occult micrometastases, provided that the optimal radionuclide is used. Our investigations on three theranostic radionuclides suggest that  $^{161}\text{Tb}$  might be a better choice than  $^{67}\text{Cu}$  or  $^{47}\text{Sc}$ . The promising characteristics of this radionuclide justify further preclinical investigations and, hopefully, clinical trials.

## Acknowledgments

We thank Pr. Keith Eckerman for helpful discussions regarding the ICRP-107 data files.

## Financial support

This work was funded by the Institut National de la Santé et de la Recherche Médicale under contract PhysiCancer "MICRONAUTE project" and by the French Investment for the Future program within LabEx TRAIL ANR-10-LABX-57.

## Competing Interests

The authors have declared that no competing interest exists.

## References

1. Volkert WA, Hoffman TJ. Therapeutic radiopharmaceuticals. Chem Rev. 1999; 99: 2269-92.
2. Mazzaferrari EL, Jhiang SM. Long-term impact of initial surgical and medical therapy on papillary and follicular thyroid cancer. Am J Med. 1994; 97: 418-28.
3. Hindri E, Mellière D, Lange F, et al. Functioning pulmonary metastases of thyroid cancer: does radioiodine influence the prognosis? Eur J Nucl Med Mol Imaging. 2003; 30: 974-81.
4. Hindri E, Zanotti-Fregonara P, Keller I, et al. Bone metastases of differentiated thyroid cancer: impact of early 131I-based detection on outcome. Endocr Relat Cancer. 2007; 14: 799-807.
5. Witzig TE, Gordon LI, Cabanillas F, et al. Randomized controlled trial of yttrium-90-labeled ibritumomab tiuxetan radioimmunotherapy versus rituximab immunotherapy for patients with relapsed or refractory low-grade, follicular, or transformed B-cell non-Hodgkin's lymphoma. J Clin Oncol. 2002; 20: 2453-63.
6. Kwekkeboom DJ, de Herder WW, Kam BL, et al. Treatment with the radiolabeled somatostatin analog [ $^{177}\text{Lu}$ -DOTA 0,Tyr3]octreotide: toxicity, efficacy, and survival. J Clin Oncol. 2008; 26: 2124-30.
7. Kratochwil C, Giesel FL, Stefanova M, et al. PSMA-targeted radionuclide therapy of metastatic castration-resistant prostate cancer with Lu-177 labeled PSMA-617. J Nucl Med. 2016; [Epub ahead of print].
8. Tolmachev V, Orlova A, Pehrson R, et al. Radionuclide therapy of HER2-positive microxenografts using a  $^{177}\text{Lu}$ -labeled HER2-specific Affibody molecule. Cancer Res. 2007; 67: 2773-82.

9. Persson M, Juhl K, Rasmussen P, et al. uPAR targeted radionuclide therapy with (177)Lu-DOTA-AE105 inhibits dissemination of metastatic prostate cancer. *Mol Pharm.* 2014; 11: 2796-806.
10. Liersch T, Meller J, Kulle B, et al. Phase II trial of carcinoembryonic antigen radioimmunotherapy with 131I-labetuzumab after salvage resection of colorectal metastases in the liver: five-year safety and efficacy results. *J Clin Oncol.* 2005; 23: 6763-70.
11. Oei AL, Verheijen RH, Seiden MV, et al. Decreased intraperitoneal disease recurrence in epithelial ovarian cancer patients receiving intraperitoneal consolidation treatment with yttrium-90-labeled murine HMFG1 without improvement in overall survival. *Int J Cancer.* 2007; 120: 2710-4.
12. Morschhauser F, Radford J, Van Hoof A, et al. Phase III trial of consolidation therapy with yttrium-90-ibritumomab tiuxetan compared with no additional therapy after first remission in advanced follicular lymphoma. *J Clin Oncol.* 2008; 26: 5156-64.
13. Witzig TE, Hong F, Micallef IN, et al. A phase II trial of RCHOP followed by radioimmunotherapy for early stage (stages I/II) diffuse large B-cell non-Hodgkin lymphoma: ECOG3402. *Br J Haematol.* 2015; 170: 679-686.
14. Price EW, Orvig C. Matching chelators to radiometals for radiopharmaceuticals. *Chem Soc Rev.* 2014; 43: 260-90.
15. Bodei L, Kidd M, Paganelli G, et al. Long-term tolerability of PRRT in 807 patients with neuroendocrine tumours: the value and limitations of clinical factors. *Eur J Nucl Med Mol Imaging.* 2015; 42: 5-19.
16. O'Donoghue JA, Bardies M, Wheldon TE. Relationships between tumor size and curability for uniformly targeted therapy with beta-emitting radionuclides. *J Nucl Med.* 1995; 36: 1902-1909.
17. Uusijärvi H, Bernhardt P, Rösck F, Maecke HR, Forsslund-Aronsson E. Electron- and positron-emitting radiolanthanides for therapy: aspects of dosimetry and production. *J Nucl Med.* 2006; 47: 807-14.
18. Hindie E, Zanotti-Fregonara P, Quinto M, Morgat C, Champion C. Dose deposits from 90Y, 177Lu, 111In, and 161Tb in micrometastases of various sizes: implications for radiopharmaceutical therapy. *J Nucl Med.* 2016; 57: 759-64.
19. DeNardo GL, Kukis DL, Shen S, DeNardo DA, Meares CF, DeNardo SJ. 67Cu-versus 131I-labeled Lym-1 antibody: comparative pharmacokinetics and dosimetry in patients with non-Hodgkin's lymphoma. *Clin Cancer Res.* 1999; 5: 533-41.
20. Knogler K, Grünberg J, Zimmermann K, et al. Copper-67 radioimmunotherapy and growth inhibition by anti-L1-cell adhesion molecule monoclonal antibodies in a therapy model of ovarian cancer metastasis. *Clin Cancer Res.* 2007; 13: 603-11.
21. Kolsky KL, Joshi V, Mausner LF, Srivastava SC. Radiochemical purification of no-carrier-added scandium-47 for radioimmunotherapy. *Appl Radiat Isot.* 1998; 49: 1541-9.
22. Müller C, Bunka M, Haller S, et al. Promising prospects for 44Sc-/47Sc-based theragnostics: application of 47Sc for radionuclide tumor therapy in mice. *J Nucl Med.* 2014; 55: 1658-64.
23. de Jong M, Breeman WA, Bernard BF, et al. Evaluation in vitro and in rats of 161Tb-DTPA-octreotide, a somatostatin analogue with potential for intraoperative scanning and radiotherapy. *Eur J Nucl Med.* 1995; 22: 608-16.
24. Müller C, Reber J, Haller S, et al. Direct in vitro and in vivo comparison of (161)Tb and (177)Lu using a tumour-targeting folate conjugate. *Eur J Nucl Med Mol Imaging.* 2014; 41: 476-85.
25. Grünberg J, Lindenblatt D, Dorrer H, et al. Anti-L1CAM radioimmunotherapy is more effective with the radiolanthanide terbium-161 compared to lutetium-177 in an ovarian cancer model. *Eur J Nucl Med Mol Imaging.* 2014; 41: 1907-15.
26. Pfeifer A, Knigge U, Binderup T, et al. 64Cu-DOTATATE PET for Neuroendocrine Tumors: A Prospective Head-to-Head Comparison with 111In-DTPA-Octreotide in 112 Patients. *J Nucl Med.* 2015; 56: 847-54.
27. Hernandez R, Valdovinos HF, Yang Y, et al. (44)Sc: an attractive isotope for peptide-based PET imaging. *Mol Pharm.* 2014; 11: 2954-61.
28. Walczak R, Krajewski S, Szklaniarz K, et al. Cyclotron production of (43)Sc for PET imaging. *EJNMMI Phys.* 2015; 2: 33.
29. Müller C, Vermeulen C, Johnston K, et al. Preclinical in vivo application of (152)Tb-DOTANOC: a radiolanthanide for PET imaging. *EJNMMI Res.* 2016; 6:35.
30. Eckerman K, Endo A. ICRP Publication 107. Nuclear decay data for dosimetric calculations. *Ann ICRP* 2008; 38: 7-96.
31. Champion C, Zanotti-Fregonara P, Hindie E. CELDOSE: a Monte Carlo code to assess electron dose distribution-S values for 131I in spheres of various sizes. *J Nucl Med.* 2008; 49: 151-7.
32. Hindie E, Champion C, Zanotti-Fregonara P, et al. Calculation of electron dose to target cells in a complex environment by Monte Carlo code "CELDOSE". *Eur J Nucl Med Mol Imaging.* 2009; 36: 130-6.
33. Champion C. Theoretical cross sections for electron collisions in water: structure of electron tracks. *Phys Med Biol.* 2003; 48: 2147-68.
34. Bardies M, Chatal JF. Absorbed doses for internal radiotherapy from 22 beta-emitting radionuclides: beta dosimetry of small spheres. *Phys Med Biol.* 1994; 39: 961-81.
35. Pantel K, Alix-Panabières C, Riethdorf S. Cancer micrometastases. *Nat Rev Clin Oncol.* 2009; 6: 339-51.
36. Braun S, Pantel K, Müller P, et al. Cytokeratin-positive cells in the bone marrow and survival of patients with stage I, II, or III breast cancer. *N Engl J Med.* 2000; 342: 525-33.
37. Bork U, Rahbari NN, Schölkopf S, et al. Circulating tumour cells and outcome in non-metastatic colorectal cancer: a prospective study. *Br J Cancer.* 2015; 112: 1306-13.
38. Aarts F, Koppe MJ, Hendriks T, et al. Timing of adjuvant radioimmunotherapy after cytoreductive surgery in experimental peritoneal carcinomatosis of colorectal origin. *Ann Surg Oncol.* 2007; 14: 533-40.
39. de Jong GM, Hendriks T, Eek A, et al. Radioimmunotherapy improves survival of rats with microscopic liver metastases of colorectal origin. *Ann Surg Oncol.* 2009; 16: 2065-73.
40. Ilan E, Sandström M, Wassberg C, et al. Dose response of pancreatic neuroendocrine tumors treated with peptide receptor radionuclide therapy using 177Lu-DOTATATE. *J Nucl Med.* 2015; 56: 177-82.
41. Chéhadé F, de Labrière-Vaylet C, Moins N, et al. Secondary ion mass spectrometry as a tool for investigating radiopharmaceutical distribution at the cellular level: the example of I-BZA and (14)C-I-BZA. *J Nucl Med.* 2005; 46: 1701-6.
42. Kassis AI. The amazing world of auger electrons. *Int J Radiat Biol.* 2004; 80: 789-803.
43. Pouget JP, Santoro L, Raymond L, et al. Cell membrane is a more sensitive target than cytoplasm to dense ionization produced by auger electrons. *Radiat Res.* 2008; 170: 192-200.
44. Aghavalian S, Boyle AJ, Reilly RM. Radioimmunotherapy of cancer with high linear energy transfer (LET) radiation delivered by radionuclides emitting  $\alpha$ -particles or Auger electrons. *Adv Drug Deliv Rev.* 2015; [Epub ahead of print].
45. Lehenberger S, Barkhausen C, Cohrs S, et al. The low-energy  $\beta$ (-) and electron emitter (161)Tb as an alternative to (177)Lu for targeted radionuclide therapy. *Nucl Med Biol.* 2011; 38: 917-24.
46. [Internet] ESTAR: Stopping-power and range tables for electrons, protons, and helium ions. <http://www.nist.gov/pml/data/star/>.